Available online at www.sciencedirect.com

ScienceDirect

Ceramics International 40 (2014) 4297–4304

CERAMICS INTERNATIONAL

www.elsevier.com/locate/ceramint

Bi-component MnO/ZnO hollow microspheres embedded in reduced graphene oxide as electrode materials for enhanced lithium storage

F. Jiang, L.W. Yang*, Y. Tian, P. Yang, S.W. Hu, K. Huang, X.L. Wei, J.X. Zhong

Hunan Key Laboratory of Micro-Nano Energy Materials and Devices, Faculty of Materials and Optoelectronic Physics, Xiangtan University, Hunan 411105, China

Received 26 June 2013; received in revised form 20 August 2013; accepted 22 August 2013
Available online 7 September 2013

Abstract

Novel composite of bi-component MnO/ZnO (denoted as MZO) hollow microspheres embedded in reduced graphene oxide (RGO) as a high performance electrode material for Lithium ion batteries (LIBs) is prepared via one-pot hydrothermal method and subsequent annealing. The structures and morphologies of as-prepared hybrid materials are characterized by X-ray diffraction, scanning electron microscopy, Raman spectra, FTIR and transmission electron microscopy. The results reveal that the MZO hollow microspheres with nanometer-sized building blocks are well dispersed in the RGO support. The electrochemical tests show that the hybrid material has a reversible capacity of 660 mAh/g at a current density of 100 mA/g with a coulombic efficiency of 98% after 100 cycles. Besides, a specific capacity of about 207 mAh/g is retained even at a current density as high as 1600 mA/g, exhibiting high reversibility and good capacity retention. Our results suggest that the composite of bi-component MZO hollow microspheres embedded in RGO will be promising electrode materials for low-cost, environmentally friendly and high-performance LIBs.

Keywords: Bi-component; Hollow microspheres; Lithium ion batteries

1. Introduction

Lithium ion batteries (LIBs) have been widely used as power sources for portable electronics in the last three decades because of their high energy density, long cycle life, and environmentally benign features [1–3]. They have also been considered to be the major player in powering pure electric vehicle (EVS) or hybrid electric vehicle (HEVS). However, their performance is fast approaching the achievable limit of currently commercial graphite electrodes [4]. This boosts a great deal of interest in seeking for high-performance electrode materials that can store and deliver more energy efficiently to replace graphite anodes. Among the available anode materials, transition metal oxides (TMOs) have always been regarded as very appealing candidates due to their higher capacity compared with commercial graphite anode (372 mA h g^{-1}), widespread availability, intrinsically enhanced safety and low processing cost. However, the practical use of these materials in LIBs has been seriously frustrated due to their poor electrical conductivity and severe electrode pulverization caused by the drastic volume variation (up to 200%) during the lithium uptake/release process[5]. Therefore, many strategies have been developed to overcome these limitations and improve the anode performance of TMOs, including increasing the specific surface area by preparing nanomaterials with various morphology and dimensions, addition of one or more electrochemically active counter atoms/ions, proper choice of the starting crystal structure, restricting the voltage range of cycling vs.Li, hybridization of bi-component TMO and so on [6–12]. There are already increasing cases that hybridization of bi-component TMO has ability to exhibit a strong synergistic effect of high capacity and remarkable rate performance on TMO electrodes, which are better than those of each component [13–16]. For example, Ahmad et al. fabricated SnO_2/ZnO

*Corresponding author. Tel.: + 8673158292195.
E-mail addresses: ylwxtu@xtu.edu.cn, ylwnju@163.com (L.W. Yang).

0272-8842/$ - see front matter © 2013 Elsevier Ltd and Techna Group S.r.l. All rights reserved.
http://dx.doi.org/10.1016/j.ceramint.2013.08.094

composite structure using a two steps hydrothermal method and reported improved reversible capacity and cycleability [13]. Li et al. reported a fabrication of $CoO/CoFe_2O_4$ nanocomposites with highly improved and tunable capacity and better cycle stability by calcination of distinctly different CoFe-LDH single-resource precursors [14]. Chen et al. synthesized rattle-type hollow structures of a-Fe_2O_3@SnO_2 and found that a-Fe_2O_3@SnO_2 nanorattles had much lower initial irreversible loss and higher reversible capacity compared to SnO_2 hollow spheres [16]. However, it is commonly challengeable to build up an integrated smart architecture using a simple and facile approach, in which structural features and synergistic effect of each component are fully manifested. Furthermore, the conductivity of these bi-component TMO hybridization electrodes is still not very satisfactory, which is important for high-performance LIBs.

Because they are more environmentally benign, much cheaper, and more abundant in nature, Mn-based binary and ternary oxides such as MnO [17,18], Mn_2O_3 [19], Mn_3O_4 [20,21], $ZnMn_2O_4$ [22] and $CoMn_2O_4$ [23] have attracted considerable interest as anode materials. Among all Mn-based oxides, MnO is one of the most attractive alternative anode materials for LIBs due to a low conversion potential, low voltage hysteresis (<0.8 V), high density (5.43 g cm^{-3}) and high specific capacity (755.6 mAh g^{-1}). However, due to its poor electric conductivity such high theoretical capacitance has not been achieved experimentally. ZnO is one of the most attractive functional semiconductor materials, which can be used as an efficient mechanical support and electron conducting pathway because of its high chemical stability, conductivity, and mechanical flexibility [24]. Although the individual LIB properties of MnO or ZnO materials have been demonstrated, there has been little study on the design and fabrication of MnO–ZnO composites as possible anode material. On the other hand, it has been demonstrated that two-dimensional graphene or reduced graphene oxide (RGO) nanosheets with superior electrical conductivity and mechanical flexibility are promising additives for anode materials of LIBs, where its major role is not only act as a conducting agent to increase the electrical conductivity of the electrode material, but also as a substrate to accommodate the volume changes and prevent the self-aggregation of the confined electrode material during the electrochemical cycling. Very recently, many types of hybrid materials consisting of graphene and electroactive materials, such as silicon, Fe_3O_4, CoO/Co_3O_4, SnO_2, $Li_4Ti_5O_{12}/TiO_2$, etc., have been successfully synthesized [25–27]. However, to the best of our knowledge, up till now there have been no reports on an electrode material integrating the advantages of ZnO, MnO and graphene or RGO in LIB anode materials.

In this work, we report the synthesis of bi-component MnO/ZnO hollow microspheres embedded in RGO (denoted as MZO/RGO) as a high performance electrode material for LIBs via one-pot hydrothermal method and subsequent annealing. The characterization of structures and morphologies reveal that the MnO/ZnO (denoted as MZO) hollow microspheres with nanometer-sized building blocks are well dispersed in the RGO support. As an anode material for LIBs, the MZO/RGO hybrid material has a reversible capacity of 660 mAh/g at a current density of 100 mA/g with a coulombic efficiency of 98% after 100 cycles. Besides, a specific capacity of about 207 mAh/g is obtained even at a current density as high as 1600 mA/g, exhibiting high reversibility and good capacity retention.

2. Experimental section

2.1. Materials synthesis

All the chemicals were of analytical grade and were used as received in all experiments. Graphene oxide (GO) was synthesized from natural graphite by a modified Hummers method [28,29]. $ZnCO_3$–$MnCO_3$ microspheres were prepared via a facile co-precipitation method. In a typical synthesis, 3.3 mmol $MnSO_4 \cdot H_2O$, 6.7 mmol $Zn(NO_3)_2 \cdot 6H_2O$ and 100 mmol $(NH_4)_2SO_4$ were dissolved in 700 mL of deionized water to form solution A. 100 mmol NH_4HCO_3 was dissolved in 700 mL of deionized water to form solution B. Then 70 mL ethanol and the solution B were sequentially poured into the solution A sequentially under vigorous stirring. Finally, the mixture was put into an oven and maintained at 50 °C for 9 h. White homogeneous $ZnCO_3$–$MnCO_3$ microspheres were collected by centrifugation, washed by deionized water and ethanol for several times, and dried at 80 °C.

The MZO/RGO hybrid material was prepared using $ZnCO_3$–$MnCO_3$ microspheres and GO as precursor via one-pot hydrothermal method and subsequent annealing as shown in Fig. 1. In a typical process, 100 mg $ZnCO_3$–$MnCO_3$ microspheres were added to 50 ml of GO suspension (2 mg/ml) under stirring. Then the mixture solution was transferred to a 100 ml Teflon-lined stainless steel autoclave and hydrothermally reacted at 180 °C for 12 h. After the reaction, the product was washed with deionized water several times. Finally the collected samples were annealed at 600 °C for 5 h under N_2 to obtain the MZO/RGO hybrid material. As a control experiment, ZnO/MnO microspheres were prepared using the same method without the addition of GO via a similar procedure.

2.2. Material characterization

The crystal structures of the synthesized samples were determined by powder X-ray diffraction (XRD) using a copper Kα radiation source ($\lambda=0.154$ nm) at 40 kV and 200 mA in steps of 0.02. Data were recorded ranging from 10° to 80°. The morphology and microstructure of the synthesized samples were characterized using scanning electron microscopy (SEM, JEOL, JSM-6490) and transmission electron microscopy (TEM, JEOL 2100) equipped with selected area electron diffraction (SAED) and an Oxford energy dispersive X-ray spectroscopy (EDS) system. Raman spectra were recorded on a Renishaw in Via system with a laser operating at $\lambda=532$ nm as excitation source. Fourier transform infrared (FT-IR) spectra measurements were carried out on a FTS-3000 Fourier transform infrared spectrophotometer.

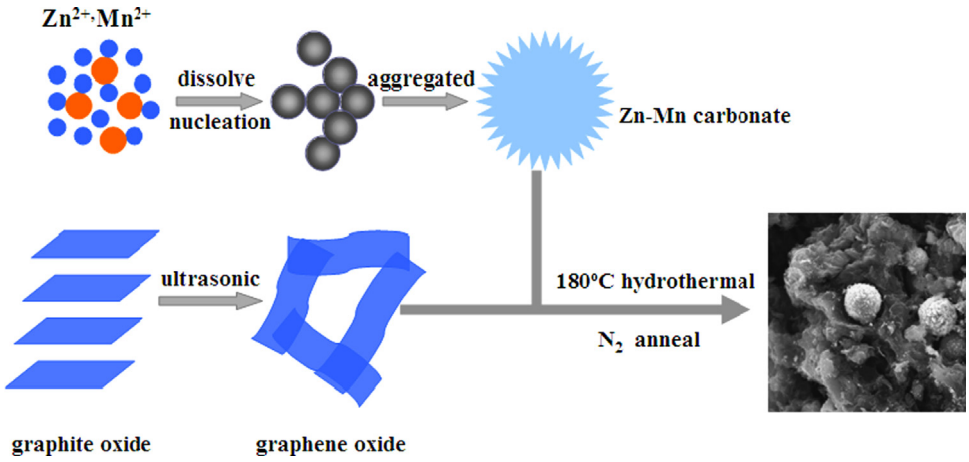

Fig. 1. Synthesis illustration of MZO/RGO hybrid material.

2.3. Electrochemical characterization

The electrochemical tests were measured using two-electrode CR2032 type coin cells.Working electrodes were prepared by pasting a mixture of the active material (MZO/RGO, MZO, and pure MnO), carbon black and polyvinylidene fluoride (PVDF) at a weight ratio of 80:10:10 onto Cu foil which acted as a current collector. The electrodes were dried at 80 °C for 6 h in air, and then at 120 °C in vacuum for another 12 h and pressed. The mass of every electrode was weighed accurately using an electronic balance. The mass of the active materials was controlled in the range of 1–2 mg. Coin cells were assembled in an argon-filled gloved box with metallic lithium foil as the counter electrode, 1 M $LiPF_6$ in ethylene carbonate (EC)/dimethyl carbonate (DEC) (1:1, volume ratio) as electrolyte, and Celgard 2400 polypropylene as separator. The charge/discharge measurements were performed at various current densities over a voltage range of 0.01–3 V (vs Li/Li^+) using a multi-channel battery test system (NEWARE BTS-610). Cyclic voltammetry (CV) measurements were carried out on an electrochemical workstation (CHI660D) in the voltage range of 0.01–3 V vs Li/Li^+ at a scan rate of 1 mV/s.

3. Results and discussions

The as prepared samples were firstly characterized by XRD, Raman and FTIR measurements. Fig. 2 depicts the XRD patterns of the as-synthesized samples. All the diffraction peaks of MZO can be well indexed according to cubic MnO (JCPDS Card no. 07-0230, space group: Fm-3 m (225), $a=b=c=4.445$ Å, $\alpha=\beta=\gamma=90°$) and hexagonal ZnO (JCPDS Card no. 36-1451, space group: P63 mc (186), $a=b=3.24982$ Å, $c=5.20661$, $\alpha=\beta=90°$, $\gamma=120°$). In contrast to MZO, a broad peak located about 26°, which belong to RGO, appears in the MZO/RGO hybrid materials. No other obvious peak located at 12.4° corresponding to an interlayer spacing of (002) in GO can be observed. The results suggest that GO has been completely transformed into RGO via the hydrothermal process [30].

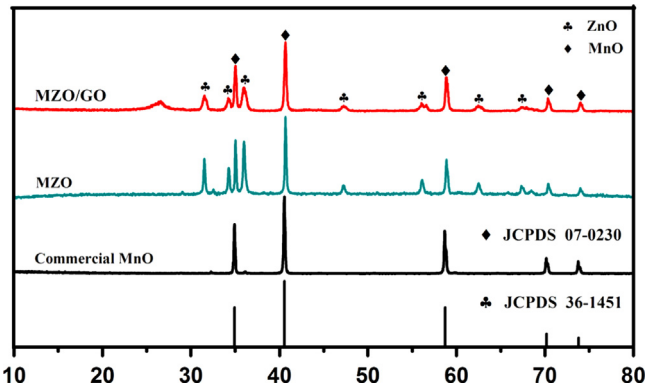

Fig. 2. XRD patterns of (a) commercial MnO, (b) MZO hollow microspheres and (c) MZO/RGO hybrid material.

Fig. 3a shows Raman spectra of the MZO/RGO and MZO composite. The characteristic D and G bands observed in the MZO/RGO composite at 1346 and 1586 cm^{-1} are in good correspondence with the reported values in the literature, respectively [31,32]. The D band is associated with disordered samples or graphene edges, while the G band is the result of the first-order scattering of the E_{2g} mode of sp^2 carbon domains. Especially, one strong Raman band at 519 cm^{-1}, which is similar with that of MZO, was observed. This characteristic Raman peak is attributed to Mn-related vibration, which can be often observed in ZnO materials with high doping Mn concentration [33]. The strong vibrational band at 648 cm^{-1} and bands below 400 cm^{-1} belong to Mn_3O_4 rather than MnO, since MnO transforms into Mn_3O_4 easily because of a local heating effect and photochemically induced transformations under beam irradiation when the beam intensity is more than 1.1 mW during the Raman measurement [34]. In addition, two obvious longitudinal optical (LO)-phonon peaks at 558 cm^{-1} (1LO) and 1052 cm^{-1} (2LO) are observed, demonstrating that multiphonon resonant process for ZnO particles in MZO/RGO samples occurs [35]. Fig. 3b shows the FITR spectra of GO and MZO/RGO composite. The transmission peaks at 3411, 1734, 1626, 1211, 1055 cm^{-1} in

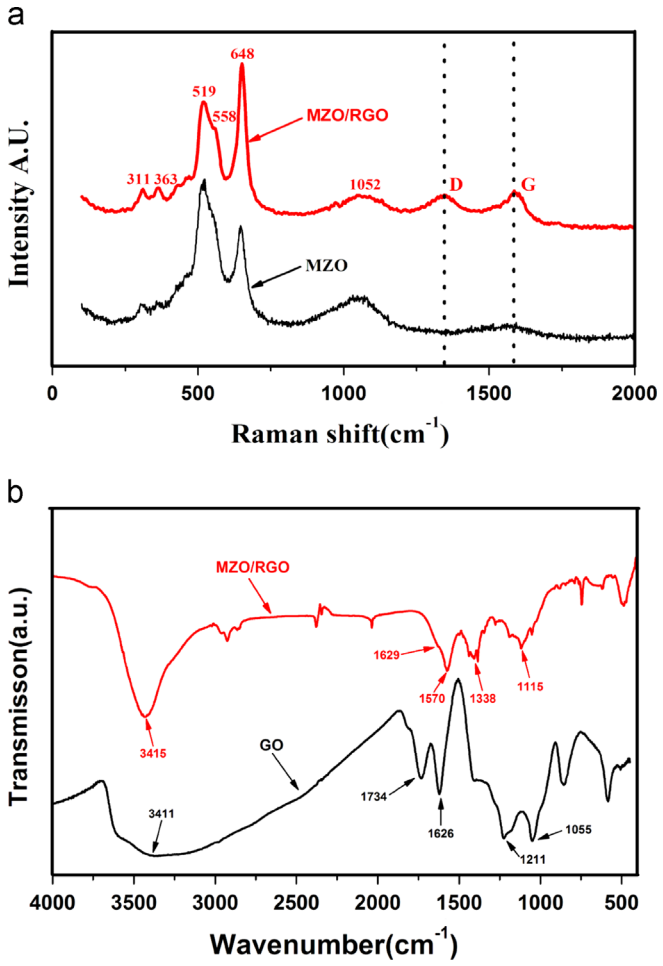

Fig. 3. (a) The Raman spectra of GO and MZO/RGO hybrid material and (b) FTIR spectra of GO and MZO/RGO hybrid material.

the FITR spectra of GO are attributed to O–H stretching vibrations, C=O stretching vibrations from carbonyl and carboxylic groups, skeletal vibrations from unoxidized graphene domains, C–OH stretching vibrations and C–O stretching vibrations, respectively [36]. Obviously, these transmission peaks disappeared or are largely decreased in MZO/RGO sample after hydrothermal treatment and subsequent annealing. The results indicate that the eliminatation of carboxyl and epoxy functional groups and the transformation of GO to RGO in MZO/RGO sample. The FTIR signals at 1338 cm^{-1} and 1115 cm^{-1} correspond to O–H bending from hydroxyl/phenol groups and C–O stretching. Interestingly, two new peaks at 1629 cm^{-1} and 1570 cm^{-1} appear, reflecting the skeletal vibration of RGO sheets [37,38]. The Raman and FTIR results confirm that the MZO/RGO sample contain RGO sheets, MnO and ZnO, which is consistent with the XRD results.

The morphology and microstructure of the samples were further examined by SEM, TEM and high-resolution TEM (HRTEM) observations. Fig. 4a and b shows the SEM images of MZO sample with different magnifications, demonstrating uniform spheres in the range of 3∼4 μm. The surface of MZO microspheres is quite rough and the nanosized building blocks can be clearly observed under higher magnifications. This interesting structure offers large interfacial area, enabling better diffusion kinetics for lithium storage to enhance the capacitive performance [23]. Fig. 4c and d shows typical SEM images of MZO/RGO hybrid material, demonstrating that the morphology of MZO microspheres can be perfectly retained without noticeable variation. In particular, one can see that the MZO microspheres are well-dispersed embedded in RGO matrix. A representative broken microsphere is also shown in Fig. 4d, where the hollow interior can be identified unambiguously from the broken part. Fig. 4e shows typical TEM image of single MZO microsphere. The hollow interior of the microspheres is clearly revealed by the sharp contrast between the center and the edge in the TEM image. The high-resolution TEM image in Fig. 4f shows the interface between MnO and ZnO. The lattice fringes having an interlayer distance of 0.256 nm and 0.192 nm agree well with the spacing between (111) planes of MnO crystals and (102) planes of ZnO crystals [39,40], respectively. Further EDS results reveal that the hollow ZMO microspheres consist of Zn^{2+} and Mn^{2+} ions and the distribution of Zn^{2+} and Mn^{2+} ions is homogeneous (see Fig. 4h), while the matrix only contained carbon (see Fig. 4i) proving that the matrix is RGO. The surrounding RGO matrix is beneficial to buffering the large volume variation of anode materials based on the conversion reaction during Li^+ insertion/extraction, thus partly mitigating the quick capacity fading issue.

To investigate the electrochemical performance of MZO/RGO hybrid material, the as-prepared compound is evaluated by CV and galvanostatic charge–discharge cycling. CV measurements were performed in order to determine the reduction potential (first cycle and subsequent cycles) and the oxidation potential of the MZO/RGO hybrid material. Fig. 5a shows representative CV traces of the first to five cycles of half-cells made using the MZO/RGO hybrid material as active materials at scan rate of 1 mV s^{-1} in the potential window between 0.01 V and 3 V versus Li/Li^+. One can find that the CV traces are similar, but not completely consistent with those of pure ZnO (see the inset) and MnO (see Supplementary Fig. 1). The results reveal that both ZnO and MnO are electroactive in MZO/RGO electrode. The CV trace of MZO/RGO electrode for the first cycle is substantially different from those of the subsequent ones. In the first cycle, a main cathodic peak are observed at 0.013 V, corresponding to the formation of solid electrolyte interface (SEI) layers and the reduction of Mn^{2+} and Zn^{2+} to metallic Mn and Zn [39,41]. In the second cycle onward, the main reduction peak is shifted to 0.48 V suggesting an irreversible phase transformation. In the cathodic process the anodic peak at 1.32 V is ascribed to the regeneration of MnO and ZnO nanograins [39,41]. The positions of oxidation peaks for the electrodes are almost unchanged, indicating the highly reversible conversion reaction of MZO/RGO composite. In addition, the CV results also reveal that MZO contributes most of the capacity for lithium storage, while the electrochemically inactive RGO serves as mechanical support and electron conducting pathway in the MZO/RGO electrodes.

Fig. 5b shows the first, second, 20th, 50th and 100th charge–discharge curves of the MZO/RGO electrodes at a

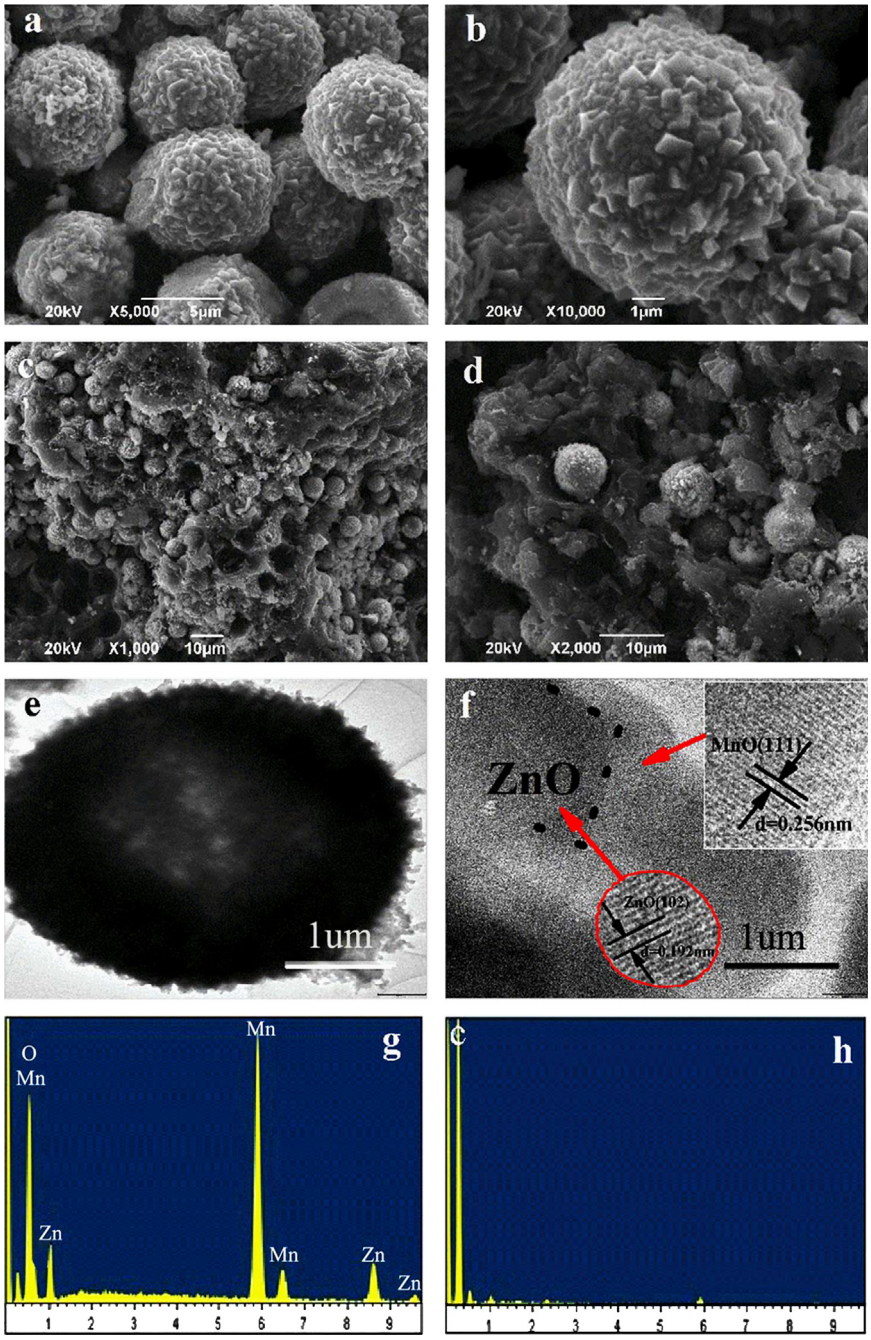

Fig. 4. SEM images of the as-synthesized (a–b) MZO hollow microspheres; (c–d) MZO/RGO hybrid material; (e–f) TEM images of MZO/RGO hybrid material and (g–h) EDS spectra of the MZO/RGO hybrid material.

current density of 100 mA g^{-1}. There exists a long voltage plateau near 0.5 V for the electrode in the first discharge cycle, but it disappears in the subsequent cycles. This phenomenon reflects the initial irreversible capacity loss which is mainly due to the formation of a SEI film [42]. The initial discharge and charge capacities of the MZO/RGO hybrid electrode are 1955 and 1146 mA h g^{-1}, respectively, which lead to an irreversible capacity loss of 809 mA h g^{-1} and low coulombic efficiency of 60%. The large irreversible capacity loss arising during the first cycle is likely to be due to the incomplete decomposition of Li_2O and the difficult dissolution of the SEI [43]. Although the coulombic efficiency of the 1st cycle is low, it is improved greatly upon cycling. For example, during the second cycle, a discharge capacity of 1146 mA h g^{-1} and a charge capacity of 1047 mA h g^{-1} are exhibited, indicating an increased coulombic efficiency of 92.06%. At the 10th cycle, the value increases to 97.47% and at the 100th cycle, it is close to 100%. Fig. 5c shows the cycling performance of the MZO/RGO, MZO and MnO electrodes. The cycling performance of MZO/RGO hybrid material was superior to those of MZO and pure MnO. After 100 cycles, a high charge capacity of 660 mA h g^{-1} for MZO/RGO hybrid material can be retained

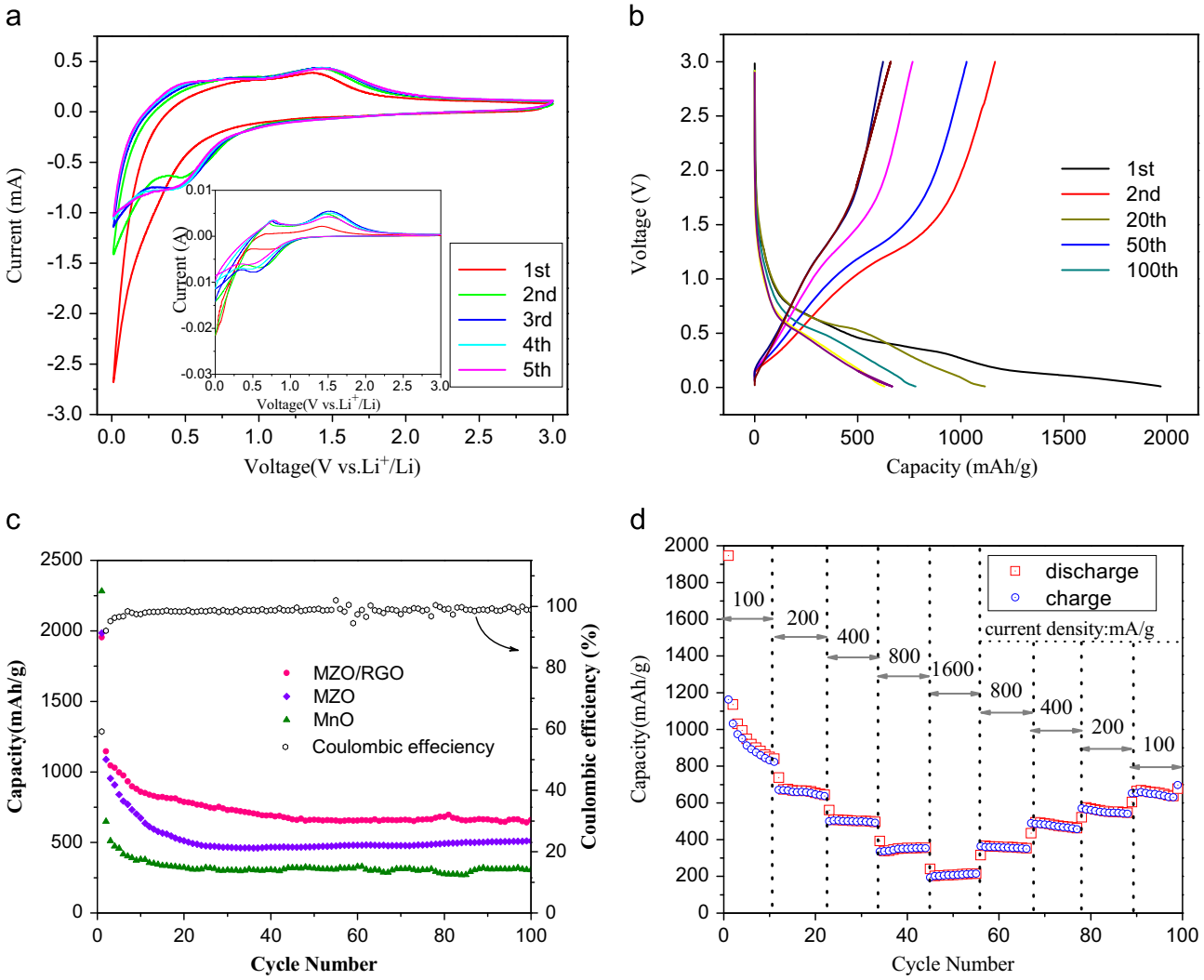

Fig. 5. (a) The first to five consecutive CVs of the MZO/RGO electrodes at a scan rate of 1 mV s^{-1} in the voltage range of 0.01–3.00 V versus Li^+/Li. The inset shows the typical CVs of the ZnO electrode; (b) Charge and discharge profiles at 100 mA g^{-1} of the MZO/RGO electrodes; (c) cycling performance; (d) rate performance of the MZO/RGO electrodes.

at a current density of 100 mA g^{-1}, which reaches that MnO/C core–shell nanorods anode material reported by Sun et al. [44]. It is worth noting that the capacity is much higher than that of graphite (372 mA h g^{-1}). Besides the high specific capacity and good cyclability, the rate capability is also a very important property for electrode materials. To evaluate the rate capability, the sample of MZO/RGO electrode is cycled at various current densities (100–1600 mA g^{-1}) and the results are shown in Fig. 5d. It is clear that the MZO/RGO sample shows excellent high rate capability at each rate. For example, at high current rate of 1600 mA g^{-1}, MZO/RGO still delivers a favorable reversible capacity of 207 mA h g^{-1} and exhibits good capacity retention, implying the efficient solid-state diffusion of lithium in MZO/RGO hybrid material. More importantly, after the high rate charge–discharge cycles, an average discharge capacity of as high as 660 mA h g^{-1} can be still maintained when the current density is gradually reduced to 100 mA/g, suggesting a good structural stability of the MZO/RGO electrode.

The above results indicate apparently the positive effect of integrated smart architecture of MZO/RGO hybrid material on the electrochemical performance. From above SEM and TEM results, it is clearly validate that the as-prepared MZO/RGO hybrid material is a combination of hollow structure, spherical morphology with nanosized building blocks and surrounding RGO sheets. First, additive electroactive ZnO acts as an efficient mechanical support and electron conducting pathway to improve the stability and anode performance of MZO/RGO electrodes. Secondly, the nanosized building blocks on the surface of MZO microspheres provide high contact area between electrolyte and electrode which is the key to improve the capacity, while the hollow characteristic of MZO microspheres accommodate the strain induced by the volume change during the electrochemical reaction which is also important to keep the structural integrity of the electrode materials. Thirdly, the surrounding RGO matrix not only act as a conducting agent, but as a substrate to accommodate the volume changes of the embedded MZO microspheres during the electrochemical cycling, thereby slowing down electrode pulverization of the

electrode materials. As a result, MZO/RGO hybrid material exhibits high capacity, good cycling and improved rate capability.

4. Conclusions

In summary, novel composite of bi-component MZO hollow microspheres embedded in RGO as a high performance electrode material for LIBs is prepared via one-pot hydrothermal method and subsequent annealing. The characterization of structures and morphologies reveals that the MZO hollow microspheres have nanometer-sized building blocks on the surface and are well-dispersed embedded in the RGO support. The hollow structure, spherical morphology with nanosized building blocks and surrounding RGO sheets of MZO/RGO hybrid material provide high contact area between electrolyte and electrode, efficient electron conducting pathway, perfect protection against the volume changes of anode materials and excellent electrical conductivity of the overall electrode during electrochemical processes. As an anode material for LIBs, compared with those of MZO and pure MnO, MZO/RGO hybrid material exhibits superior anode performance including high capacity, good cycling and improved rate capability.

Acknowledgments

This work was supported by the Grants from National Natural Science Foundation of China (No. 51272220, 11275163, 11204262, and 11374252), National Basic Research Program of China (2012CB921303), the Open Fund based on the innovation platform of Hunan colleges and universities (No.12K045) and Scientific Research Fund of Hunan Provincial Education Department (No. 13C926).

Appendix A. Supporting information

Supplementary data associated with this article can be found in the online version at http://10.1016/j.ceramint.2013.08.094.

References

[1] J.M. Tarascon, M. Armand, Issues and challenges facing rechargeable lithium batteries, Nature 414 (2001) 359–367.
[2] J. Hassoun, P. Reale, B. Scrosati, Recent advances in liquid and polymer lithium-ion batteries, Journal of Materials Chemistry 17 (2007) 3668–3677.
[3] R. Koksbang, J. Barker, H. Shi, M.Y. Saïdi, Cathode materials for lithium rocking chair batteries, Solid State Ionics 84 (1996) 1–21.
[4] Y. Deng, S. Tang, Q. Zhang, Z. Shi, L. Zhang, S. Zhan, G. Chen, Controllable synthesis of spinel nano-$ZnMn_2O_4$ via a single source precursor route and its high capacity retention as anode material for lithium ion batteries, Journal of Materials Chemistry 21 (2011) 11987–11995.
[5] Z. Wang, Z. Wang, W. Liu, W. Xiao, X.W. Lou, Amorphous $CoSnO_3$@C nanoboxes with superior lithium storage capability, Energy and Environmental Science 6 (2013) 87–91.
[6] I.A. Courtney, J. Dahn, Electrochemical and in situ X-ray diffraction studies of the reaction of lithium with tin oxide composites, Journal of the Electrochemical Society 144 (1997) 2045–2052.
[7] H. Li, X. Huang, L. Chen, Anodes based on oxide materials for lithium rechargeable batteries, Solid State Ionics 123 (1999) 189–197.
[8] H. Uchiyama, E. Hosono, I. Honma, H. Zhou, H. Imai, A nanoscale meshed electrode of single-crystalline SnO for lithium-ion rechargeable batteries, Electrochemistry Communications 10 (2008) 52–55.
[9] Z.P. Guo, G.D. Du, Y. Nuli, M.F. Hassan, H.K. Liu, Ultra-fine porous SnO_2 nanopowder prepared via a molten salt process: a highly efficient anode material for lithium-ion batteries, Journal of Materials Chemistry 19 (2009) 3253–3257.
[10] H. Liu, D. Long, X. Liu, W. Qiao, L. Zhan, L. Ling, Facile synthesis and superior anodic performance of ultrafine SnO_2-containing nanocomposites, Electrochimica Acta 54 (2009) 5782–5788.
[11] J.S. Chen, X.W. Lou, One-pot synthesis of carbon-coated SnO_2 nanocolloids with improved reversible lithium storage properties, Electrochemistry Communications 11 (2009) 2332–2335.
[12] Z. Chen, Y. Cao, J. Qian, X. Ai, H. Yang, Facile synthesis and stable lithium storage performances of Sn- sandwiched nanoparticles as a high capacity anode material for rechargeable Li batteries, Journal of Materials Chemistry 20 (2010) 7266–7271.
[13] M. Ahmad, S. Yingying, H. Sun, W. Shen, J. Zhu, SnO_2/ZnO composite structure for the lithium-ion battery electrode, Journal of Solid State Chemistry 196 (2012) 326–331.
[14] M. Li, Y.-X. Yin, C. Li, F. Zhang, L.-J. Wan, S. Xu, D.G. Evans, Well-dispersed bi-component-active CoO/$CoFe_2O_4$ nanocomposites with tunable performances as anode materials for lithium-ion batteries, Chemical Communications 48 (2012) 410–412.
[15] M.F. Hassan, M.M. Rahman, Z. Guo, Z. Chen, H. Liu, SnO_2–NiO–C nanocomposite as a high capacity anode material for lithium-ion batteries, Journal of Materials Chemistry 20 (2010) 9707–9712.
[16] J.S. Chen, C.M. Li, W.W. Zhou, Q.Y. Yan, L.A. Archer, X.W. Lou, One-pot formation of SnO_2 hollow nanospheres and Fe_2O_3@SnO_2 nanorattles with large void space and their lithium storage properties, Nanoscale 1 (2009) 280–285.
[17] K. Zhong, B. Zhang, S. Luo, W. Wen, H. Li, X. Huang, L. Chen, Investigation on porous MnO microsphere anode for lithium ion batteries, Journal of Power Sources 196 (2011) 6802–6808.
[18] X.Q. Yu, Y. He, J.P. Sun, K. Tang, H. Li, L.Q. Chen, X.J. Huang, Nanocrystalline MnO thin film anode for lithium ion batteries with low overpotential, Electrochemistry Communications 11 (2009) 791–794.
[19] Y. Qiu, G.-L. Xu, K. Yan, H. Sun, J. Xiao, S. Yang, S.-G. Sun, L. Jin, H. Deng, Morphology-conserved transformation: synthesis of hierarchical mesoporous nanostructures of Mn_2O_3 and the nanostructural effects on Li-ion insertion/deinsertion properties, Journal of Materials Chemistry 21 (2011) 6346–6353.
[20] J. Gao, M.A. Lowe, H.D. Abruña, Spongelike nanosized Mn_3O_4 as a high-capacity anode material for rechargeable lithium batteries, Chemistry of Materials 23 (2011) 3223–3227.
[21] H. Wang, L.-F. Cui, Y. Yang, H. Sanchez Casalongue, J.T. Robinson, Y. Liang, Y. Cui, H. Dai, Mn_3O_4 − graphene hybrid as a high-capacity anode material for lithium ion batteries, Journal of the American Chemical Society 132 (2010) 13978–13980.
[22] L. Zhou, H.B. Wu, T. Zhu, X.W. Lou, Facile preparation of $ZnMn_2O_4$ hollow microspheres as high-capacity anodes for lithium-ion batteries, Journal of Materials Chemistry 22 (2012) 827–829.
[23] L. Zhou, D. Zhao, X.W. Lou, Double-shelled $CoMn_2O_4$ hollow microcubes as high-capacity anodes for lithium-ion batteries, Advanced Materials 24 (2012) 745–748.
[24] H. Pang, Y. Ma, G. Li, J. Chen, J. Zhang, H. Zheng, W. Du, Facile synthesis of porous ZnO–NiO composite micropolyhedrons and their application for high power supercapacitor electrode materials, Dalton Transactions 41 (2012) 13284–13291.
[25] S. Han, D. Wu, S. Li, F. Zhang, X. Feng, Graphene: a two-dimensional platform for lithium storage, Small 9 (2013) 1173–1187.
[26] Y. Sun, Q. Wu, G. Shi, Graphene based new energy materials, Energy and Environmental Science 4 (2011) 1113–1132.
[27] Z.-S. Wu, G. Zhou, L.-C. Yin, W. Ren, F. Li, H.-M. Cheng, Graphene/metal oxide composite electrode materials for energy storage, Nano Energy 1 (2012) 107–131.

[28] W.S. Hummers, R.E. Offeman, Preparation of graphitic oxide, Journal of the American Chemical Society 80 (1958) (1339–1339).
[29] S. Stankovich, R.D. Piner, S.T. Nguyen, R.S. Ruoff, Synthesis and exfoliation of isocyanate-treated graphene oxide nanoplatelets, Carbon 44 (2006) 3342–3347.
[30] M. Sathish, S. Mitani, T. Tomai, A. Unemoto, I. Honma, Nanocrystalline tin compounds/graphene nanocomposite electrodes as anode for lithium-ion battery, Journal of Solid State Electrochemistry 16 (2012) 1767–1774.
[31] L.M. Malard, M.A. Pimenta, G. Dresselhaus, M.S. Dresselhaus, Raman spectroscopy in graphene, Physics Reports 473 (2009) 51–87.
[32] A.C. Ferrari, J.C. Meyer, V. Scardaci, C. Casiraghi, M. Lazzeri, F. Mauri, S. Piscanec, D. Jiang, K.S. Novoselov, S. Roth, A.K. Geim, Raman Spectrum of Graphene and Graphene Layers, Physical Review Letters 97 (2006) 187401.
[33] L.W. Yang, X.L. Wu, G.S. Huang, T. Qiu, Y.M. Yang, In situ synthesis of Mn-doped ZnO multileg nanostructures and Mn-related Raman vibration, Journal of Applied Physics 97 (2005) 014308.
[34] I. Rusakova, T. Ould-Ely, C. Hofmann, D. Prieto-Centurión, C.S. Levin, N.J. Halas, A. Lüttge, K.H. Whitmire, Nanoparticle shape conservation in the conversion of MnO nanocrosses into Mn_3O_4, Chemistry of Materials 19 (2007) 1369–1375.
[35] Y. Zhu, H.I. Elim, Y.L. Foo, T. Yu, Y. Liu, W. Ji, J.Y. Lee, Z. Shen, A.T. S. Wee, J.T.L. Thong, C.H. Sow, Multiwalled carbon nanotubes beaded with ZnO nanoparticles for ultrafast nonlinear optical switching, Advanced Materials 18 (2006) 587–592.
[36] S. Stankovich, D.A. Dikin, R.D. Piner, K.A. Kohlhaas, A. Kleinhammes, Y. Jia, Y. Wu, S.T. Nguyen, R.S. Ruoff, Synthesis of graphene-based nanosheets via chemical reduction of exfoliated graphite oxide, Carbon 45 (2007) 1558–1565.
[37] P. Lian, X. Zhu, S. Liang, Z. Li, W. Yang, H. Wang, Large reversible capacity of high quality graphene sheets as an anode material for lithium-ion batteries, Electrochimica Acta 55 (2010) 3909–3914.
[38] W. Chen, L. Yan, In situ self-assembly of mild chemical reduction graphene for three-dimensional architectures, Nanoscale 3 (2011) 3132–3137.
[39] Y.J. Mai, D. Zhang, Y.Q. Qiao, C.D. Gu, X.L. Wang, J.P. Tu, MnO/reduced graphene oxide sheet hybrid as an anode for Li-ion batteries with enhanced lithium storage performance, Journal of Power Sources 216 (2012) 201–207.
[40] A. Bragaru, M. Kusko, E. Vasile, M. Simion, M. Danila, T. Ignat, I. Mihalache, R. Pascu, F. Craciunoiu, Analytical characterization of engineered ZnO nanoparticles relevant for hazard assessment, Journal of Nanoparticle Research 15 (2012) 1–17.
[41] H. Wanga, Q. Pan, Y. Cheng, J. Zhao, G. Yin, Evaluation of ZnO nanorod arrays with dandelion-like morphology as negative electrodes for lithium-ion batteries, Electrochimica Acta 54 (2009) 2851–2855.
[42] M.-S. Wu, H.-W. Chang, Self-Assembly of NiO-coated ZnO nanorod electrodes with core–shell nanostructures as anode materials for rechargeable lithium-ion batteries, The Journal of Physical Chemistry C 117 (2013) 2590–2599.
[43] W. Yao, J. Yang, J. Wang, Y. Nuli, Multilayered cobalt oxide platelets for negative electrode material of a lithium-ion battery, Journal of the Electrochemical Society 155 (2008) A903–A908.
[44] B. Sun, Z. Chen, H.-S. Kim, H. Ahn, G. Wang, MnO/C core–shell nanorods as high capacity anode materials for lithium-ion batteries, Journal of Power Sources 196 (2011) 3346–3349.